

A Combined Multi-Technique In Situ Approach Used to Probe the Stability of Iron Molybdate Catalysts During Redox Cycling

Matthew G. O'Brien · Andrew M. Beale ·
Simon D. M. Jacques · Bert M. Weckhuysen

Published online: 18 June 2009

© The Author(s) 2009. This article is published with open access at Springerlink.com

Abstract A setup combining a number of techniques (WAXS, XANES and UV–Vis) has been used to probe the stability of an iron molybdate catalyst during redox cycling. The catalyst was first reduced under anaerobic methanol/helium conditions, producing formaldehyde and then regenerated using air. Although in this test-case the catalyst and conditions differ from that of a commercial catalyst bed we demonstrate how such a setup can reveal new information on catalyst materials. In particular we observe the formation of two phases during reduction; one which we propose to be an oxygen deficient ‘pseudo-molybdate phase’, the other a molybdenum carbide-like phase, both produced as oxygen is removed from the catalyst. Standard in situ techniques could detect such transient phases, however, the information from multiple techniques, allows us to more accurately identify the nature of these materials and to carry out appropriate complementary ex situ measurements to aid in the analysis. This and similar setups therefore offer a way to more quickly and accurately observe reaction

pathways within a catalyst, which may for example, result in the deactivation of the material by different routes to those observed previously. Additionally, the specific combination of these techniques with on-line mass spectrometry, allows us to monitor the activity of the catalyst surface and here observe that different catalytic mechanisms may occur during different stages of the redox process. Therefore this setup should allow for the observation of many novel variations in a catalyst’s reactivity, leading to the improvement of current and development of new materials.

Keywords Multi-technique in situ · WAXS · XANES · UV–Vis · Iron molybdate · Methanol to formaldehyde · Catalyst deactivation

1 Introduction

An understanding of the reaction and deactivation processes of catalytic systems is vitally important for the development and improvement of many industrial processes. The use of synchrotron light sources has, for a number of decades now, provided a way to examine catalysts under increasingly more realistic conditions [1–6]. The continued development of more brilliant and powerful light sources along with improved detectors has more recently allowed for the combination of two and three X-ray based in situ techniques [1, 7–12]. Information can now be collected on various parts of the catalyst congruently revealing additional insight into their operation under various conditions.

To demonstrate the power of this approach, we have studied a ‘model’ stoichiometric iron molybdate (FeMo) catalyst under ‘accelerated’ (anaerobic) conditions, allowing changes to be measured within the timescale available for a synchrotron experiment [13]. In situ combined wide-

Electronic supplementary material The online version of this article (doi:10.1007/s11244-009-9324-z) contains supplementary material, which is available to authorized users.

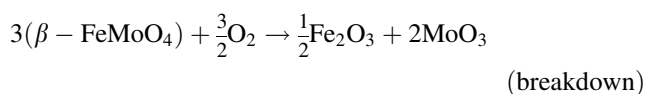
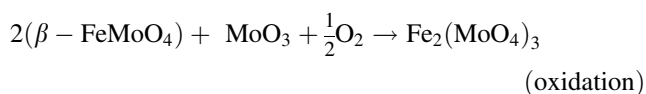
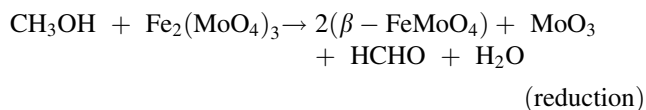
M. G. O'Brien · A. M. Beale · B. M. Weckhuysen (✉)
Inorganic Chemistry and Catalysis Group, Debye Institute for
Nanomaterials Science, Utrecht University, Sorbonnelaan 16,
3584 CA Utrecht, The Netherlands
e-mail: b.m.weckhuysen@uu.nl

S. D. M. Jacques
Department of Chemistry, University College London,
20 Gordon Street, London WC1H 0AJ, UK

S. D. M. Jacques
Department of Crystallography, Birkbeck College, Industrial
Materials Group, University of London, WC1E 7HX London,
UK

angle X-ray scattering (WAXS), X-ray absorption near edge spectroscopy (XANES) and ultraviolet–visible (UV–Vis) spectroscopy with online mass spectrometry (MS) was used to monitor the structure–activity relationships during reduction/oxidation cycles of a solid catalyst.

Commercial FeMo catalysts are used for the production of formaldehyde from methanol by oxidative dehydrogenation, operating under relatively mild conditions (~ 350 °C) with a long lifetime (up to 2 years). The $\text{Fe}_2(\text{MoO}_4)_3$ phase is generally considered to be the primary active phase, and, under standard conditions, a partial reduction of this phase occurs on reaction with methanol, resulting in the formation of formaldehyde, inactive $\beta\text{-FeMoO}_4$ and MoO_3 [14]. These are then rapidly regenerated to $\text{Fe}_2(\text{MoO}_4)_3$ by oxygen in the gas stream completing the catalytic cycle. However, under these conditions sublimation of molybdenum can occur, particularly at reactor hot spots and, if there is not sufficient excess molybdenum in the catalyst (i.e. if Mo/Fe is not greater than 1.5), breakdown to oxides occurs [13, 15–18]:



Many authors believe the redox process occurs via a Mars–Van Krevelen type mechanism, [14, 19–21]. This mechanism is supported by kinetic studies and experimental works indicating rapid diffusion of bulk oxygen to the catalyst surface [22–27]. However, some measurements indicate that the process can also be expressed using modified Langmuir–Hinshelwood kinetics (with and without oxygen participation) [28, 29].

In this work we examine the behavior of an $\text{Fe}_2(\text{MoO}_4)_3$ catalyst under redox conditions. Whilst these conditions ultimately differ from those used during normal operation of the catalyst, they have been used to regenerate commercial pelletized systems after deactivation and can still provide useful information into the catalysts behavior under extreme conditions [30]. These experiments then allow us to demonstrate the potential of the multiple-technique approach (in conjunction with complementary ex situ characterization) to improve our understanding of the chemical processes in catalysts. Here we identify the formation of intermediate phases and examine the surface reaction mechanism. In particular we note how the measurement of congruent changes provides details not readily available from single in

situ technique methods, allowing us to more readily identify forming species and deactivation pathways.

2 Experimental

2.1 Sample Preparation and Characterization

$\text{Fe}_2(\text{MoO}_4)_3$ (Mo/Fe = 1.5:1) is generally synthesized via co-precipitation or sol–gel methods. However, here batch hydrothermal were used at temperatures far lower than those employed in previous works, following similar procedures to those recently used to produce inorganic and organo-metallic iron molybdates [31–35].

The products were initially characterized ex situ by powder diffraction using a Bruker D8 X-ray diffractometer (Co source, $K_{\alpha 1}$ 1.78897 Å) in the Bragg–Brentano orientation and fitted with a rotating flat plate to reduce preferred orientation. A typical diffraction pattern is given in the supplementary information (S1) and indexed to the $\text{Fe}_2(\text{MoO}_4)_3$ structure with a P1211 symmetry [36]. The Bruker D8 was also used during the ‘quenching’ experiment on the P1 phase. Energy dispersive X-ray analysis (EDX) was performed using a Jeol 733 Superprobe with an Oxford Instruments ISIS/INCA system and indicated the Mo:Fe to be 1.5:1. The high quality scan of the P2 phase (used here ‘ex situ’) was obtained from a separate in situ experiment performed under identical conditions on station 6.2 at the SRS (UK) using a rapid accumulation (10 s^{-1} /scan) time at a wavelength of 1.4 Å [37].

Temperature programmed calcination and gas chromatography (GC) experiments were performed using an Interscience compact GC fitted with both flame ionization (Carboxen micropacked and HayesepQ packed columns) and thermal conductivity (capillary PorabondQ column) detectors.

2.2 In Situ Techniques

Combined in situ experiments were performed using WAXS, XANES and UV–Vis techniques on the DUBBLE beamline (BM26A) at the European synchrotron radiation facility (ESRF), Grenoble, France, operating at 6 GeV with a peak current of 200 mA. X-ray absorption spectra were recorded at the Mo K-edge (19999.5 eV—calibrated using a 20 μm molybdenum foil) in transmission mode using a Si (111) double-crystal monochromator, followed by two vertically focusing Pt- and Si-coated mirrors for harmonic rejection. An ion chamber was used for measuring incident beam intensities, whilst the transmitted signal was recorded using an ODD-15W photodiode mounted within a SAXS tube (not utilized in these measurements). A typical collection rate of 3 min/scan was employed.

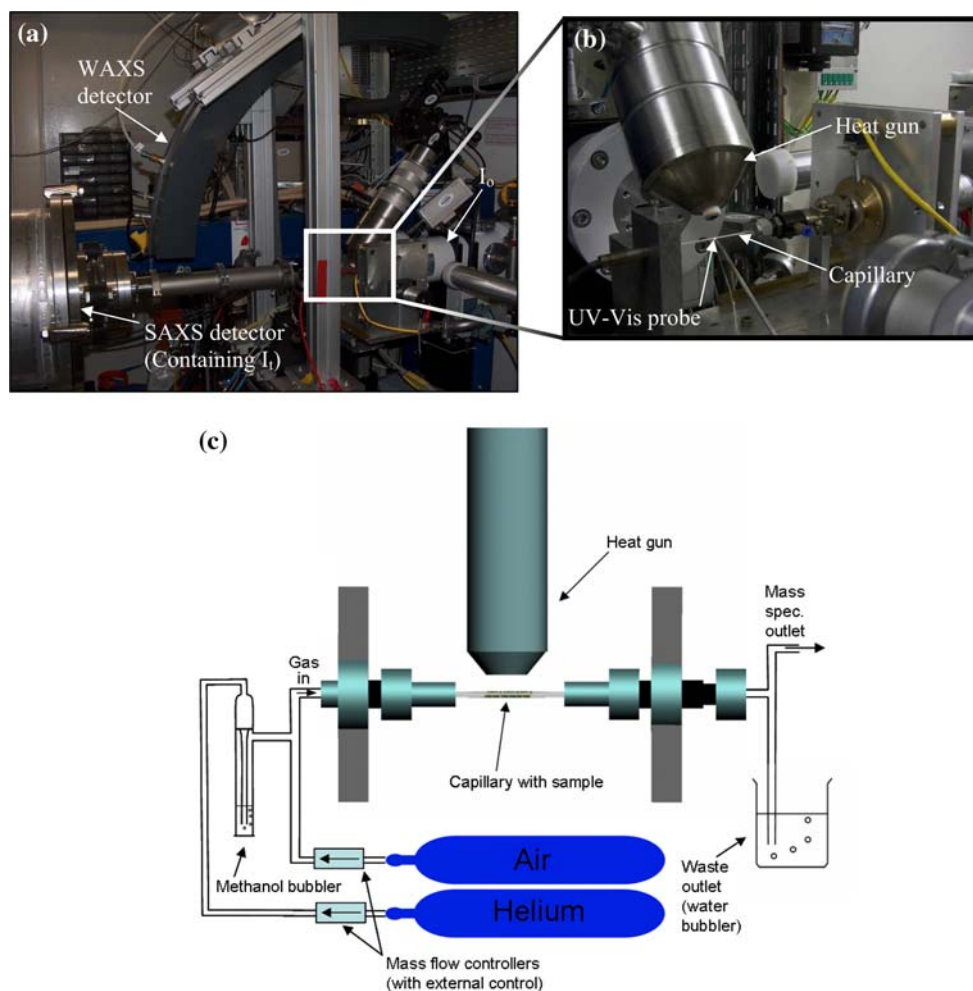
WAXS patterns were recorded sequentially after the XANES using an angular dispersive multi-channel INEL detector, below the Mo K-edge at 17658.98 eV ($\lambda = 0.702104 \text{ \AA}$). A silicon standard was used to calibrate the detector and data was collected at a rate of 3 min/scan. Thus an overall collection time of 7 min was employed for the XANES/WAXS collection sequence (including an additional 1 min of ‘dead time’ due to monochromator motor movement). Diffuse reflectance UV–Vis spectra were measured using a 600 μm optical fiber probe connected to both an Avantes AVS-SD2048 spectrometer and a Halogen Deuterium light source. As this part of the setup is independent of the beam line optics a greater acquisition rate of 1 min/scan was used. MS traces were recorded using a European Spectrometry Systems (ESS) ecoSys-P Man-Portable mass spectrometer with a capillary inlet and heated inlet tube.

The experiments were performed using an experimental setup similar to that described previously, however heat was supplied from a hot air gun rather than a block furnace [38]. The setup is detailed in Fig. 1, indicating the position of the heat gun, WAXS detector, XANES ions chambers (I_0 and I_t) and the UV–Vis probe in relation to the sample

capillary ($\phi = 0.7 \text{ mm}$ quartz). Note that although the SAXS detector was not used in these experiments it does offer the possibility of combining an additional technique to this setup. The figure also demonstrates the gas flow system with the reducing MeOH/He mix supplied via a bubbler resulting in a methanol saturation in the gas phase of $\sim 15\%$ (based on the vapor pressure of methanol at 21 $^\circ\text{C}$) [39]. Air grade zero was supplied directly to the catalyst for oxidation and the rate of both gasses was controlled using mass flow devices, triggered by 5v TTL pulses from outside the experimental hutch.

Typically the sample was heated to 350 $^\circ\text{C}$ at 5 $^\circ\text{C}/\text{min}$ under a highly reducing MeOH/He mix at a flow rate of 50 mL/min. After 26 min at temperature the gas was switched to air to regenerate the catalyst, then further MeOH/He (from 77 min at temp.) and air (from 110 min at temp.) stages were performed. Although these ‘accelerated aging’ conditions were far more extreme than a commercial iron molybdate catalyst will encounter they allow us to demonstrate the ability of this setup to observe and identify phase changes in a catalyst which may not be observed using ex situ techniques [13]. Additionally, heating the

Fig. 1 View of the combined in situ setup demonstrating the positions of the WAXS detector and the incident (I_0) and transmission (I_t) ion chambers for XAS in relation to the sample environment (note that the SAXS tube was not used in these experiments but did house I_t) **a** a close up of the environmental cell demonstrating the position of the heat gun and the UV–Vis probe, **b** and a schematic of the setup illustrating the gas flow through the experimental cell **(c)**



sample during methanol flow should result in an increased chance to observe transient phases formation within the time frame of the techniques and provide detail of how this material operates at lower temperatures.

2.3 Data Analysis

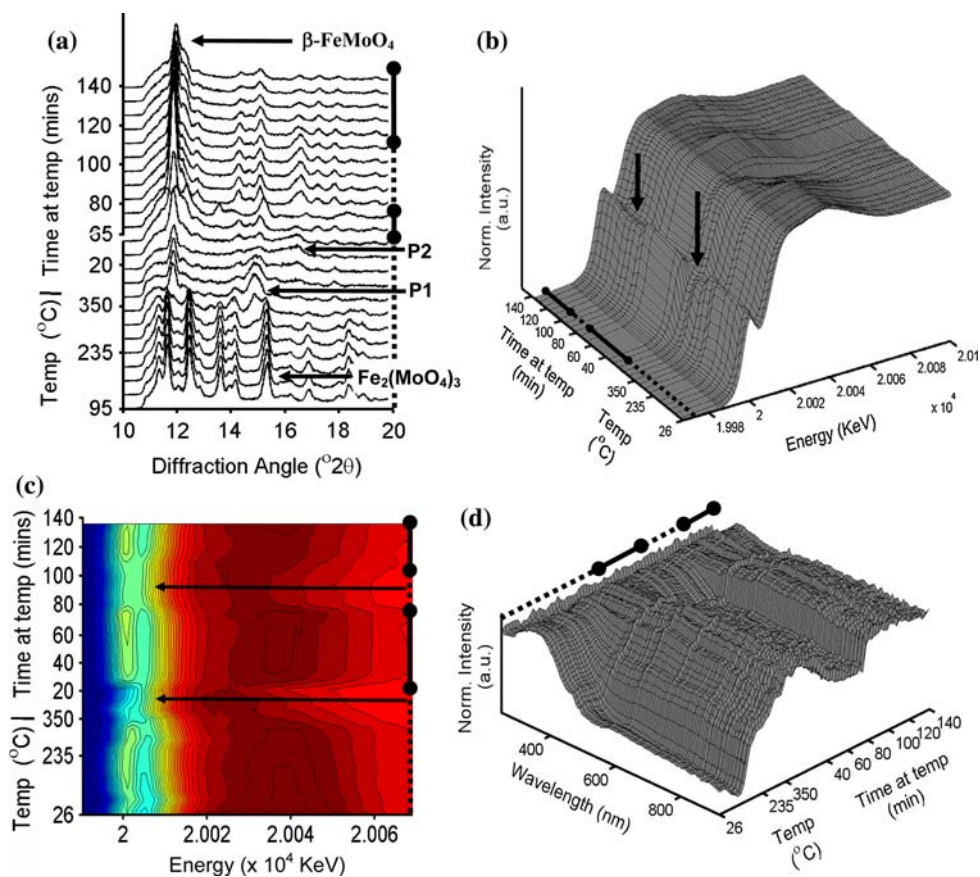
Due to the large number of (often) complex crystalline phases formed during the redox process, peak intensity fits rather than a full Rietveld analysis was used to determine the contribution of each phase at each point. Prior to XANES analysis the data were converted to 2 column ASCII and normalized using in-house multiple conversion macros. The area of the pre-edge peak was then measured using a spline to extract it from the rest of the XANES signal and then fitting was performed using a standard Gaussian peak fitting routine. UV–Vis data was converted to ASCII using Avantes Incorporated Avasoft software v 7.0.3 and normalized to a reference point at which there was no UV–Vis signal (in this case 250 nm) using in-house Matlab (revision 2007(a)) macros. MS data were converted to ASCII using Pfeiffer vacuum's Quadstar-32 bit conversion program. Traces for formaldehyde, methanol, dimethyl ether (DME) and CO₂ were measured. For formaldehyde a trace at m/z 30 was used as these changes can be mainly attributed to the parent ion.

However, some methanol ion contribution was also observed and this was corrected using the methanol molecular ion signal. The parent ion of methanol (m/z 32) was not observed and therefore methanol conversion was determined from the signal for the molecular ion (m/z 31), whilst the parent ions for both DME (m/z 46) and CO₂ (m/z 44) were used. Due to the very strong nitrogen signal from air, CO production could not be reliably monitored. We note that during the formation of the various oxides it is possible that volatile molybdenum species may also form. However, due to the temperature of the MS transfer line (100 °C) such materials would condensate before the detector and therefore not be detected by this setup.

3 Results

In Fig. 2 we plot the informative parts of the raw data obtained from each of the techniques used in this experiment, from which considerable changes are observed during the redox cycles. The WAXS data (Fig. 2a) shows that the initial Fe₂(MoO₄)₃ phase (full peak assignments are given in supplementary information S1) converted to the inactive β-FeMoO₄ and MoO₂ (as the MoO₃ was rapidly reduced) during reduction. It was then partially regenerated

Fig. 2 In situ time and temperature-resolved data collected from the multiple technique setup on the FeMo catalyst. In all cases *dashed lines* represent reduction whilst *solid lines* represent oxidation. WAXS (a) shows the formation of two unexpected phases (labeled P1 and P2) during reduction whilst XANES (b) shows a significant decrease in the Mo pre-edge feature (*arrows*). A contour plot of the XANES (c) also reveals shifts in both the edge and post-edge features to lower energies (*arrows*) whilst a clear darkening of the sample during reduction is observed by UV–Vis (d)



during the first oxidation cycle but in the second oxidation little or no regeneration occurred, indicating total catalyst breakdown. Interestingly, two transient phases, previously un-observed during $\text{Fe}_2(\text{MoO}_4)_3$ reduction (labeled P1 and P2), formed at a temperature of $\sim 260^\circ\text{C}$ (shoulder at $14.85^\circ 2\theta$) and $\sim 340^\circ\text{C}$ (broad peak centered at $16.4^\circ 2\theta$), respectively. A contour plot of this data also demonstrates the presence of these phases and shows that the peaks were not due to a simple shift in the $\text{Fe}_2(\text{MoO}_4)_3$ phase during heating (supplementary information S2). Additionally, amorphization of the rest of the sample during the formation of P1 and P2 was noted.

The XANES data given in Fig. 2b indicates a reversible decrease in the Mo pre-edge during both reduction cycles; however, this was far more significant during the first reduction. A contour plot of this data (Fig. 2c) then reveals that there were also shifts in both the edge and post-edge features towards lower energies, indicating that an oxidation or coordination state change (or both) occurred at the same time. Finally, from an initial UV–Vis pattern (supplementary information S3) and the stack data given in Fig. 1d, we note two prominent bands. The first is a ligand to metal charge transfer band (LMCT) which dominated the UV region (350 nm) and remained throughout the reaction. The second is a sharp (but weak) band (463 nm) which appeared to be characteristic of the $\text{Fe}_2(\text{MoO}_4)_3$ phase (although its exact origin remains unknown) and disappeared as the temperature increased above $\sim 175^\circ\text{C}$ [40, 41]. The stack plot also indicates that the absorbance (particularly in the visible region) generally increased during reduction and then decreased during oxidation. However, as the experiment proceeded this variation became less pronounced, with the sample remaining more absorbing.

To obtain more details on these changes and how they relate to each other, a more thorough analysis was performed. For clarity we initially detail these plots and then discuss the changes. Figure 3 plots the intensities of the phases observed in the WAXS data as a function of temperature/time, allowing for a more accurate comparison as to when each phase is formed and how they are related to each other (although we note that WAXS data can be insensitive to very low concentrations of material resulting in some small time variation). In Fig. 4 we measure the change in the area of the Mo pre-edge feature to profile the changes initially observed in Fig. 2b throughout the reaction. A quantitative in situ measurement of the shift of the edge and post-edge positions observed in the contour plot was not possible, however a comparison at the beginning and end of the initial reduction (supplementary information S4) clearly indicates the shift was towards lower energies. In Fig. 5 we plot the absorbance of the UV–Vis signal in the visible region and although there was little change in

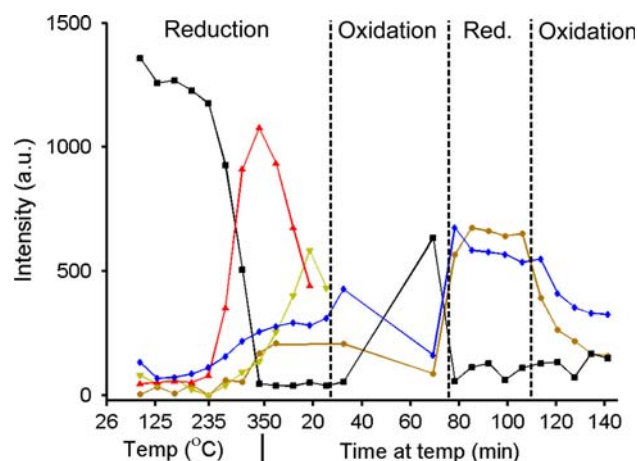


Fig. 3 A plot of the WAXS intensity of the various phases present in the FeMo catalyst throughout the redox reaction cycles (—■— $\text{Fe}_2(\text{MoO}_4)_3$, —▲— P1, —▼— P2, —◆— $\beta\text{-FeMoO}_4$, —●— MoO_2). $\text{Fe}_2(\text{MoO}_4)_3$ intensity was measured from the peak at $13.59^\circ 2\theta$, P1 at $14.89^\circ 2\theta$, P2 at $16.41^\circ 2\theta$, $\beta\text{-FeMoO}_4$ at $13.59^\circ 2\theta$ and MoO_2 at $16.5^\circ 2\theta$. Note that due to significant peak overlap it was impossible to measure MoO_2 between 70 and 98 min, as at this point it is directly correlated with the formation of unidentified phase 2 (P2)

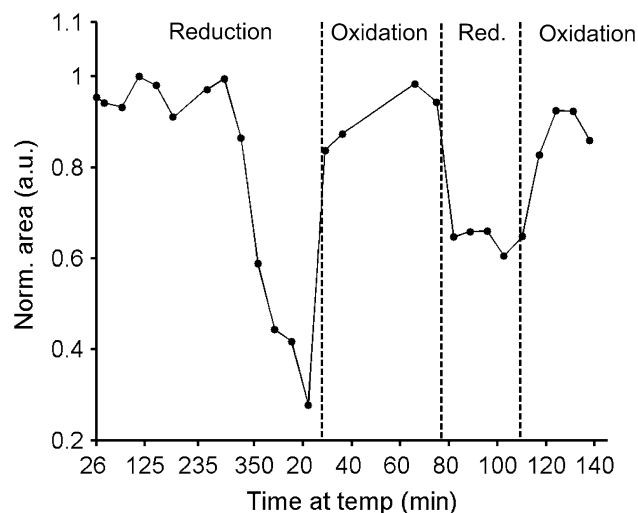


Fig. 4 The normalized XANES pre-edge intensity recorded as a function of temperature and time

the rest of the spectrum, this measurement provides useful information on the sample color and therefore the redox state of the material. The plot confirms a general darkening of the sample during reduction and brightening during oxidation, which was much reduced during the second redox cycle. Interestingly, we also noted an initial (until $\sim 130^\circ\text{C}$) decrease in intensity. As this could not be due to the sample getting lighter, we believe it was a result of some initial settling as the experimental cell/sample expands during heating.

In Fig. 6 we show the MS traces for formaldehyde (a), methanol (b), DME (c) and CO_2 (d) to allow for structure

activity relationships to be observed. Formaldehyde production was observed when the sample reached $\sim 260^\circ\text{C}$ and levels off as the sample reached temperature (i.e. $350^\circ\text{C}/0\text{ min at temp.}$). The methanol concentration initially decreased during heating and first reduction, indicating some initial retention on the surface of the catalyst. This then leveled off after formaldehyde production began. Interestingly, there was a sharp increase in formaldehyde production during switching between gases. For the oxidation to reduction switch this occurred in two steps with an initial spike then a broader increase followed by a decrease (observed more clearly in supplementary information S5). DME was observed in small quantities in the reaction (from acid sites within the catalyst [42, 43]), and

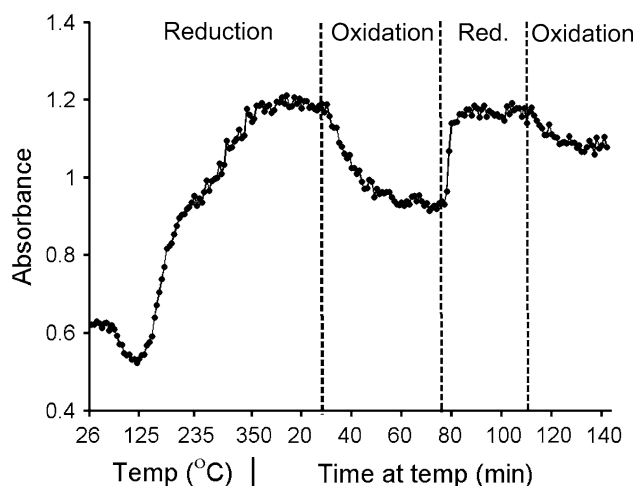


Fig. 5 Measurement of the UV-Vis absorbance at 675 nm as a function of temperature and time

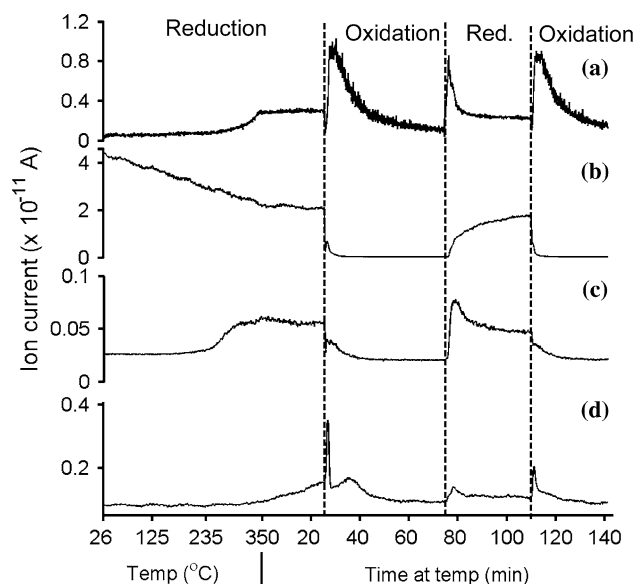


Fig. 6 Mass spec traces for formaldehyde (a), methanol (b), DME (c) and CO_2 (d) as a function of temperature and time

formed just prior to initial formaldehyde at a lower temperature of $\sim 235^\circ\text{C}$ and generally followed a similar trend, although with smaller ‘spikes’ during gas switching. CO_2 was also observed and again followed the same general trends as formaldehyde. However, its initial production occurred later than that of formaldehyde. Additionally, during both switches from reduction to oxidation, there were very large spikes, followed by more gradual increase/decrease. These were noted to be stronger during the first redox cycle.

Finally, to aid in the analysis, a number of complementary ex situ measurements were recorded. In Fig. 7 a high quality ex situ scan of a sample quenched during the reduction process is given, from which a more detailed assignment of the P1 phase was possible (Table 1). In Fig. 8 a similar scan of the P2 phase is given. In Fig. 9 we display GC analysis from a temperature programmed oxidation of a sample quenched during the reduction stage, from which both CO and CO_2 , were observed forming.

4 Discussion

4.1 Phase Formation

By comparing this data it is now possible to begin to identify the phases formed in the catalyst (particularly P1 and P2) and analyze the effect of redox cycles on the material.

During the first reduction, the expected conversion of the catalyst from the active $(\text{Fe}_2(\text{MoO}_4)_3)$ to the inactive $(\beta\text{-FeMoO}_4)$, phase and MoO_3 (reduced to MoO_2) was observed to begin at $\sim 200^\circ\text{C}$. However, two phases (P1

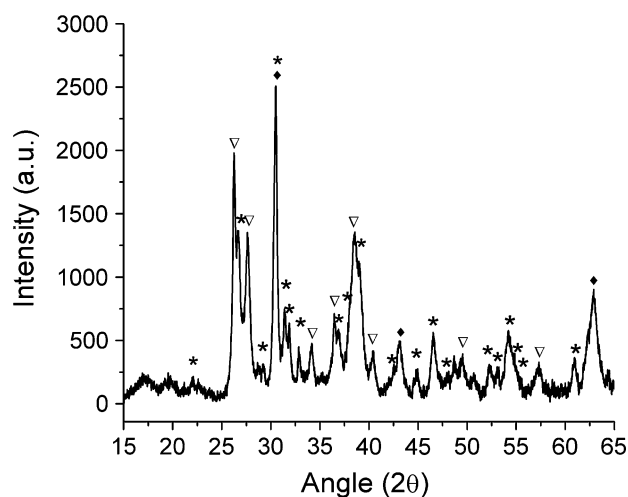
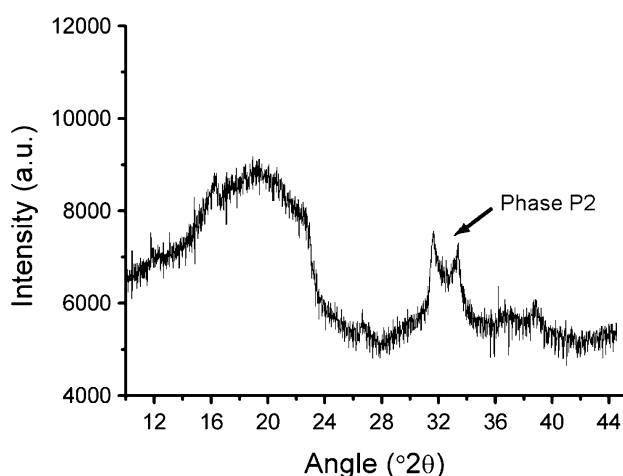


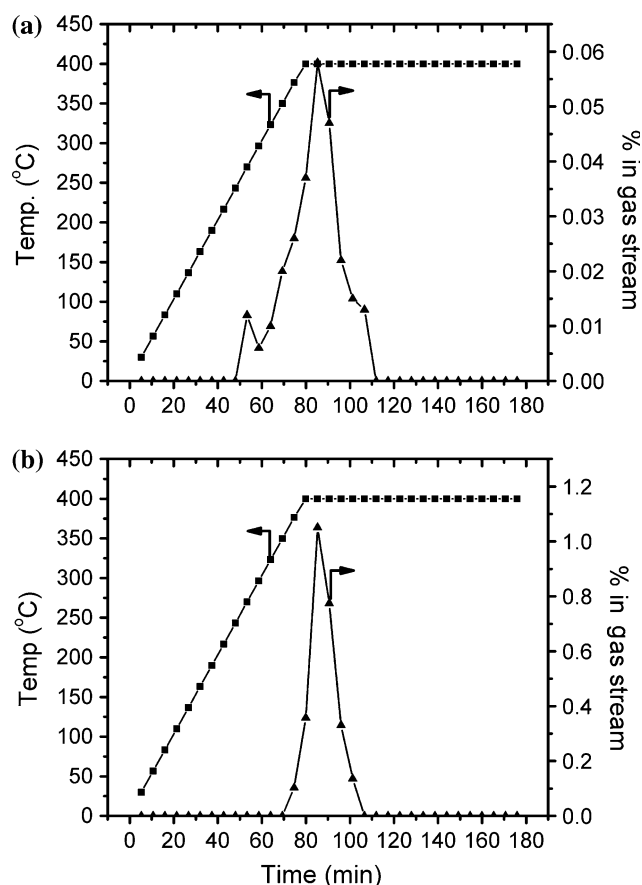
Fig. 7 Ex situ XRD pattern of the reduced FeMo catalyst quenched during P1 formation, a number of peaks of which are clearly observed (inverted triangle). At this stage the sample also contains $\beta\text{-FeMoO}_4$ (asterisk) and MoO_2 (filled diamond)

Table 1 The list of peaks identified for the P1 phase determined from ex situ X-ray diffraction

d spacing	2θ ($\lambda = 1.7889 \text{ \AA}$)	2θ ($\lambda = 0.7021 \text{ \AA}$)
3.93855	26.25	10.23
3.749269	27.61	10.75
3.043689	34.18	13.25
2.859615	36.46	14.11
2.707894	38.58	14.90
2.58912	40.42	15.86
2.134564	49.55	18.93
1.86523	57.31	21.70

**Fig. 8** A scan taken of the P2 phase during reduction using a rapid data recording experimental setup ($\lambda = 1.4 \text{ \AA}$)

and P2) were also observed to form. It was not possible from the in situ WAXS data to identify the P1 phase and, whilst an ex situ scan revealed considerable more detail, positive identification using scattering techniques alone was not possible. However, a combination of the time resolved WAXS with XANES data gave more insight into its nature. Both the P1 and $\beta\text{-FeMoO}_4$ phases formed as $\text{Fe}_2(\text{MoO}_4)_3$ was consumed, although some $\beta\text{-FeMoO}_4$ continues forming after $\text{Fe}_2(\text{MoO}_4)_3$ and P1 is consumed. This suggests that, although some $\text{Fe}_2(\text{MoO}_4)_3$ may be converted directly to $\beta\text{-FeMoO}_4$, under these conditions a large portion is actually initially converted to P1. Therefore P1 may be some intermediate leading to the reduced phases and this is supported by the XANES which shows a small change in the pre-edge intensity during P1 formation. This $1s \rightarrow 4d$ electronic transition is sensitive to the both the geometry and oxidation state of the Mo environment. Considering that both $\text{Fe}_2(\text{MoO}_4)_3$ and $\beta\text{-FeMoO}_4$ contain similar Mo environments it seems likely that any intermediate phase would also contain a similar Mo environment and that this small decrease in the pre-edge intensity can be attributed to the formation of the MoO_2 [44, 45]. At

**Fig. 9** The evolution of CO (a) and CO_2 (b) from a reduced sample of the catalyst during a temperature programmed calcination. For both gases peak output was observed when the temperature of the experiment has reached a maximum of $400 \text{ }^\circ\text{C}$

this stage formaldehyde production is occurring (Fig. 6a) demonstrating that formaldehyde oxidation must be occurring via a Mars–Van Krevelen mechanism with oxygen being supplied from the lattice. From these observations we can propose that P1 is an oxygen deficient/reduced intermediate derived from $\text{Fe}_2(\text{MoO}_4)_3$. It can then convert to $\beta\text{-FeMoO}_4$ via a rearrangement of the crystalline structure whilst maintaining the overall Mo environment. Indeed, such ‘pseudo-molybdate’ phases are not uncommon and have been observed in similar systems during the accumulation of vacancies in the crystal lattice [46–48]. However, despite the ex situ XRD revealing the phase in more detail it was not possible to fully index P1 to any known crystalline material, indicating therefore it is most likely a variant of these.

Although a quantitative comparison of the intensity of different phases in the WAXS was not possible (i.e. the amount of $\beta\text{-FeMoO}_4$ formed from $\text{Fe}_2(\text{MoO}_4)_3$ during reduction) we do note that the amount of $\text{Fe}_2(\text{MoO}_4)_3$ regenerated on oxidation was only about half of that expected. This indicates that although this ‘pseudo-

molybdate' phase is an intermediate in the formation of β -FeMoO₄, under these conditions the conversion was interrupted and another phase must be formed from P1. This was confirmed by the presence of the second phase (P2) observed in the WAXS.

P2 appeared after P1 and continued to grow as P1 diminished; thus it appears that P2 also forms from P1. This phase gave few peaks in the diffraction and, like P1, cannot be identified from this technique alone. However, when combined with the other in situ and complementary ex situ techniques more insight can be revealed. For example, a significant reduction in the XANES pre-edge feature and a shift in the edge position and post edge features towards lower energies occurred at this stage. This can be partly attributed to the formation of MoO₂, however, during the second reduction there was clearly far more MoO₂ formed (WAXS) but this resulted only in a small change in the XANES. Therefore we rationalize that the significant changes in the XANES during this first reduction were not primarily attributable to MoO₂ but to the P2 phase which also formed at this time. It is clear then that although P2 is weakly diffracting, it was present in significant quantities during this stage of the reduction. The Mo environment of P2 is therefore significantly different compared to tetrahedral Mo⁶⁺ containing Fe₂(MoO₄)₃ and β -FeMoO₄ and has both a lower oxidation and possibly a different coordination state. Ex situ high quality diffraction data then revealed the P2 phase to be similar to molybdenum carbide (MoC) [49–51]. These peak positions do not exactly match those described previously, however, this is not surprising given the complex nature of the MoC system, and indicates the formation of a MoC variant [51]. This assignment is also consistent with the weak pre-edge observed in the XANES (typical of lower oxidation state containing Mo compounds) and the darkening of the catalyst as seen by UV–Vis (although we observe that MoO₂ and coke formation will also contribute to this) [52–54]. MoC type material formation is also supported by the complementary ex situ oxidation of a pre-reduced sample in a GC where considerable quantities of CO and CO₂ were released, most likely as a result of MoC breakdown. Finally, considering the mass spectrum data, we note that formaldehyde production continued throughout P2 formation indicating continued oxygen removal from the catalyst. Therefore, by again combining the observations from multiple in situ techniques and using complementary ex situ observations, we can now propose that P2 is a form of molybdenum carbide. It is formed from P1 as oxygen is continually extracted from the bulk to supply surface production of formaldehyde and represents a more complete breakdown of the catalyst. Such a conclusion would appear reasonable as similar materials have been observed in both unsupported iron molybdate and Mo supported zeolites [55–59].

Interestingly, we note that rather than cause complete deactivation as observed here, anaerobic methanol conditions have actually been used to regenerate these catalysts [30]. This however can be explained by the fact that, in those previous studies, a slow deactivation of a pelletized catalyst resulted in a molybdenum rich bulk with a deficient surface. Regeneration then occurred by migration of the bulk molybdenum to the surface. Here the use of a stoichiometric powder under rapidly reducing conditions causes a 'deeper' reduction of the entire material, resulting in a catalyst with no unaffected bulk which consequently cannot then be regenerated.

Indeed, during the first oxidation P2 disappeared immediately but only about half of the original Fe₂(MoO₄)₃ was recovered. This was accompanied by both an increase in the Mo pre-edge peak intensity and a spike in CO₂ production; this being consistent with the decomposition of MoC (although it may also be partly due to the oxidation of surface bound methoxy species). Therefore rather than regeneration, the catalyst undergoes a breakdown towards poorly crystalline Mo oxide phase(s) (in addition to MoO₃—WAXS signal at 12.36° 2 θ). During the second oxidation the amount of this poorly crystalline appeared to increase since the original Fe₂(MoO₄)₃ phase did not recover during the time frame of the experiment (although we observe this may be a kinetic phenomenon since further experiments on similar sample indicate that with extended time periods Fe₂(MoO₄)₃ can reform) [37]. Therefore, the buildup of poorly crystalline Mo-containing oxides within the system resulted in a material that could not be easily regenerated. Although these phases and their production do differ from those produced during regeneration of the commercial catalyst, these results do indicate how a lack of additional molybdenum and a deep reduction can result in the breakdown of iron molybdate.

Although the final poorly crystalline Mo-oxide phases could not be directly identified, such species are not uncommon and have been observed in similar catalyst materials [48, 60–65]. In addition, the breakdown of the catalyst should result in iron sub-oxides (during reduction) and iron oxides (oxidation) [13, 30]. These are also not directly observed, however their presence can be inferred by the increase in CO₂ production during reduction as these phases are well known to catalyze methanol total oxidation [66, 67].

It is also important to note that during the second reduction neither P1 nor P2 were observed. As P1 is an intermediate its formation and conversion is most likely too rapid (at this higher (isothermal) temperature) to be observed within the time resolution of the experiment. For P2 however, we note that during the second reduction the majority of the remaining Fe₂(MoO₄)₃ was converted to β -FeMoO₄. This indicates that P2 formation may be

temperature dependant and does not form/or is less stable at higher temperatures, as observed in recent studies [37].

4.2 Catalyst Activity

Whilst the multiple technique data allows us to observe changes in the catalyst structure during redox cycling, details regarding the catalytic mechanism at the catalyst surface can also be gleaned from the online mass spectrum data in Fig. 6. Indeed, the interaction of methanol on both an oxidation catalysts surface and bulk has been well studied [42, 68, 69].

Here, we observe that formaldehyde production occurred despite the absence of oxygen, suggesting the source of oxygen for the reaction to be the catalyst bulk (Mars–Van Krevelen like process). Interestingly however, on switching to air we observed a large increase in the formaldehyde production. As there was no methanol being introduced, the source of formaldehyde is likely to be surface-bound methoxy species [25, 70, 71]. This sudden increase in formaldehyde production in the absence of $\text{Fe}_2(\text{MoO}_4)_3$ suggests that in these circumstances, the oxygen necessary to complete the reaction cycle leading to formaldehyde formation must have come directly from the gas phase. It is possible this could occur via a rapid regeneration/reduction of $\text{Fe}_2(\text{MoO}_4)_3$ in a Mars–Van Krevelen like manner, however we note that as no $\text{Fe}_2(\text{MoO}_4)_3$ was observed forming during the second oxidation, despite increased formaldehyde production, this seems unlikely. It is of course possible that during this second oxidation a surface type $\text{Fe}_2(\text{MoO}_4)_3$ phase formed, again however also seems unlikely as one would then expect this to nucleate and form observable FeMo phases as in the first oxidation. Additionally, a dissociative adsorption, rearrangement to an active phase and then rapid extraction of oxygen at active sites would most likely be a slow process, whilst the observed increase in reactivity is rapid. These results therefore suggest that a Langmuir–Hinshelwood rather than a Mars–Van Krevelen type process is occurring at this stage. This is observation is important since it suggests that both mechanisms can operate in the catalyst depending on the exact conditions and may explain the different observations in previous works [22–29]. Further evidence for this ‘dual’ mechanism can also be found from the changes in formaldehyde production on switching from back from air to methanol. Here (unlike in the methanol to air switch over) two features were observed (supplementary information S6). The sharp spike observed immediately after changing gas is most likely a result of rapid surface reaction of remaining oxygen with the methanol in a Langmuir–Hinshelwood process, whilst the second broader peak (reaching a maximum just after this spike) can be explained by continued formaldehyde production from bulk oxygen (as in the initial reduction).

5 Conclusions

In this paper we have demonstrated the use of a multiple technique approach to probe a catalytic material under redox conditions. The system used and the conditions employed where not identical to those used in a commercial catalyst system, however the setup could be easily adapted to perform such tests. The time resolved nature of the experiment demonstrates the possibility to identify intermediate phases such as P1 and/or P2, whilst the combination of WAXS, EXAFS and UV–Vis along with online MS allows us to easily and simultaneously probe the catalyst from local to long range order. This considerably increases the possibility to not only identify the formation of intermediate species but to attempt to begin to assess their nature. We also note that this work demonstrates that ex situ studies often remain essential in aiding the analysis of the in situ results, providing complementary information when required.

In the experiments performed in this test case the P1 and P2 phases were observed and then identified as being an oxygen defective intermediate pseudo-molybdate and a MoC type phase respectively, formed as oxygen is continually removed from the catalyst bulk. Interestingly, the formation of the latter appears to lead to the breakdown of the catalyst to oxides (which can then only slowly be regenerated). This differs from observations within a commercial catalyst where similar He/methanol conditions encourage migration of excess molybdenum to the catalyst surface and allow regeneration [30]. This appears to be a result of the different nature of the catalyst and conditions employed here, but does indicate that under certain conditions MoC formation may occur resulting in the breakdown of the catalyst. This test study has therefore demonstrated the power of a multiple technique approach to examine multi-component catalysts and more easily identify both new phases and alternate deactivation routes. This is important as understanding all potential deactivation routes and their conditions allow for their avoidance in the development of modified or new catalyst systems.

Additionally, we have shown how the measurement of online mass spectrum data along with WAXS can reveal important information with regard to surface activity. We have shown for example that for MoO_3 redox, both a Mars–Van Krevelen and a Langmuir–Hinshelwood type mechanism can operate. Similar measurements would be useful on catalysts operating under more operando conditions as such information is again important for the understanding and development of catalyst systems.

Acknowledgments The authors would like to thank CW-NWO for funding (VICI to BMW and VENI to AMB) and access to the DUBBLE facility (BM26A). Olivier Leynaud, Wim Bras, Sergey Nikitenko, Anna Iglesia Juez and Dirk Detollenaere are also acknowledged for their assistance in acquiring the data.

Open Access This article is distributed under the terms of the Creative Commons Attribution Noncommercial License which permits any noncommercial use, distribution, and reproduction in any medium, provided the original author(s) and source are credited.

References

- Tinnemans SJ, Mesu JG, Kervinen K, Visser T, Nijhuis TA, Beale AM, Keller DE, van der Eerden AMJ, Weckhuysen BM (2006) *Catal Today* 113:3
- Topsoe H (2003) *J Catal* 216:155
- Weckhuysen BM (2002) *Chem Commun* 97
- Weckhuysen BM (2004) *In situ spectroscopy of catalysts*. American Scientific Publishers, Stevenson Ranch
- Weckhuysen BM (2003) *Phys Chem Chem Phys* 5:4351
- Banares MA (2005) *Catal Today* 100:71
- Beale AM, van der Eerden AMJ, Jacques SDM, Leynaud O, O'Brien MG, Meneau F, Nikitenko S, Bras W, Weckhuysen BM (2006) *J Am Chem Soc* 128:12386
- Beale AM, van der Eerden AMJ, Kervinen K, Newton MA, Weckhuysen BM (2005) *Chem Commun* 3015
- Bruckner A (2003) *Catal Rev-Sci Eng* 45:97
- Brückner A (2005) *Chem Commun* 1761
- Grunwaldt JD, Molenbroek AM, Topsoe NY, Topsoe H, Clausen BS (2000) *J Catal* 194:452
- Newton MA, Burnaby DG, Dent AJ, Diaz-Moreno S, Evans J, Fiddy SG, Neisius T, Turin S (2002) *J Phys Chem B* 106:4214
- Pernicone N (1991) *Catal Today* 11:85
- Soares APV, Portela MF (2005) *Catal Rev-Sci Eng* 47:125
- Pernicone N (2003) *Cattech* 7:196
- Soares APV, Portela MF, Kiennemann A (2001) *Catal Commun* 2:159
- Burriesci N, Garbassi F, Petrera M, Petrini G, Pernicone N (1980) *Stud Surf Sci Catal* 6:115
- Andersson A, Hernelind M, Augustsson A (2006) *Catal Today* 112:40
- Mars P, Van Krevelen DW (1954) *Chem Eng Sci Spec Suppl* 3:41
- Pernicone N, Lazzarin F, Liberti G, Lanzavecchia G (1969) *J Catal* 14:293
- Pernicone N (1974) *J Less-Common Met* 36:289
- Lafyatis DS, Creten G, Froment GF (1994) *Appl Catal A Gen* 120:85
- Jiru P, Wichterlova B, Tichy J (1965) In: *Proceedings of the 3rd international congress on catalysis*, Amsterdam, vol 1, p 199
- Dente M, Poppi R, Pasquon J (1964) *Chim Ind* 46:1326
- Farneth WE, Ohuchi F, Staley RH, Chowdhry U, Sleight AW (1985) *J Phys Chem* 89:2493
- Carbucicchio M, Trifiro F (1976) *J Catal* 45:77
- Novakova J, Jiru P (1972) *J Catal* 27:155
- Bhattacharyya SK, Janakiram K, Ganguly ND (1967) *J Catal* 8:128
- Vannice MA (2007) *Catal Today* 123:18
- Wachs IE, Briand LE (2000) US Patent 6,037,290
- Klevtsov PV (1965) *Kristallografiya* 10:445
- Marshall DJ (1967) *J Mater Sci* 2:294
- Byrappa K, Yosimura M (2001) *Handbook of hydrothermal technology—technology for crystal growth and materials processing*. William Andrew Publishing/Noyes
- Beale AM, Jacques SDM, Sacaliuc-Parvalescu E, O'Brien MG, Barnes P, Weckhuysen BM (2008) *Appl Catal A Gen*. doi:10.1016/j.apcata.2009.05.008
- Ding Y, Yu SH, Liu C, Zang ZA (2007) *Chem-Eur J* 13:746
- Rapposch MH, Anderson JB, Kostiner E (1980) *Inorg Chem* 19:3531
- Jacques SDM, Leynaud O, Strusevich D, Stukas P, Barnes P, Sankar G, Sheehy M, O'Brien MG, Iglesia-Juez A, Beale AM (2008) *Catal Today* Accepted for publication. doi:10.1016/j.cattod.2009.02.012
- Jacques SDM, Leynaud O, Strusevich D, Beale AM, Sankar G, Martin CM, Barnes P (2006) *Angew Chem Int Ed* 45:445
- Weast RC (1968) *Handbook of chemistry and physics*, 49th edn. The Chemical Rubber Co, Cleveland
- Lever ABP (1984) *Inorganic Electronic Spectroscopy*. Elsevier, Amsterdam, p 531. ISBN: 0444423893
- Thomazeau C, Martin V, Afanasiev P (2000) *Appl Catal A Gen* 199:61
- Badlani M, Wachs IE (2001) *Catal Lett* 75:137
- Wachs IE, Jehng JM, Ueda W (2005) *J Phys Chem B* 109:2275
- Antonio MR, Teller RG, Sandstrom DR, Mehicic M, Brazdil JF (1988) *J Phys Chem* 92:2939
- Teo BK (1986) *EXAFS: basic principles and data analysis*. Springer-Verlag, Berlin
- Fagherazzi G, Pernicone N (1970) *J Catal* 16:321
- Mitov I, Asenov S, Tomov T, Klissurski D (2007) *J Phys Chem C* 111:5389
- Sunkou MR, Mendioroz S, Fierro JLG, Palacios JM, Guerreroruiz A (1995) *J Mater Sci* 30:496
- Fries RJ, Kempter CP (1960) *Anal Chem* 32:1898
- Matsumoto O, Yaguchi Y, Shiota Y, Kanzaki Y (1983) *High Temp Sci* 16:243
- Lu J, Hugosson H, Eriksson O, Nordström L, Jansson U (2000) *Thin Solid Films* 370:203
- Lacheen HS, Iglesia E (2005) *J Catal* 230:173
- Ding WP, Li SZ, Meitzner GD, Iglesia E (2001) *J Phys Chem B* 105:506
- Rocha AS, da Silva VT, Eon JG, de Menezes SMC, Faro AC, Rocha AB (2006) *J Phys Chem B* 110:15803
- Weckhuysen BM, Rosynek MP, Lunsford JH (1998) *Catal Lett* 52:31
- Weckhuysen BM, Wang DJ, Rosynek MP, Lunsford JH (1998) *J Catal* 175:347
- Solyosi F, Cserenyi J, Szoke A, Bansagi T, Oszko A (1997) *J Catal* 165:150
- Wang HM, Wang XH, Zhang MH, Du XY, Li W, Tao KY (2007) *Chem Mater* 19:1801
- Li XL, Li YD (2004) *Chem-Eur J* 10:433
- Magneli A (1948) *Acta Chem Scand* 2:861
- Magneli A (1948) *Acta Chem Scand* 2:501
- Chen SC, Greenblatt M (1994) *J Solid State Chem* 108:366
- Kihlberg L (1960) *Acta Chem Scand* 14:1612
- Portemer F, Sundberg M, Kihlberg L, Figlarz M (1993) *J Solid State Chem* 103:403
- Trifiro F, Notarbartolo S, Pasquon I (1971) *J Catal* 22:324
- Kolovrtnov GD, Boreskov GK, Dzisko VA, Popov BI, Tarasova DV, Belugina GC (1965) *Kinet Catal (Engl Transl)* 6:950
- Bowker M, Holroyd R, Elliott A, Morrall P, Alouche A, Entwistle C, Toerncrona A (2002) *Catal Lett* 83:165
- Tatibouet JM (1997) *Appl Catal A Gen* 148:213
- Routray K, Briand LE, Wachs IE (2008) *J Catal* 256:145
- Farneth WE, McCarron EM, Sleight AW, Staley RH (1987) *Langmuir* 3:217
- House MP, Carley AF, Echeverria-Valda R, Bowker M (2008) *J Phys Chem C* 112:4333